

Landslides (2019) 16:937–953
 DOI 10.1007/s10346-019-01144-4
 Received: 4 November 2018
 Accepted: 31 January 2019
 Published online: 27 February 2019
 © Springer-Verlag GmbH Germany
 part of Springer Nature 2019

Jiading Wang · Dengfei Zhang · Nianqin Wang · Tianfeng Gu

Mechanisms of wetting-induced loess slope failures

Abstract Frequent occurrence of landslides induced by rainfall or irrigation has seriously threatened the urban and rural development in the Loess Plateau, China. The increase in pore water pressure has been identified as a key factor for understanding wetting-induced loess slopes failures. However, experimental studies are limited regarding the increase in pore water pressure of the collapse loess from an initial negative value until failure occurs under constant total stress condition. An old landslide with progressive retreat development at an early stage of the construction of the Lvliang Airport was selected as a case study. Field surveys including exploration wells and boreholes revealed very fresh sliding shear planes and clearly visible cracks, suggesting the creeping movement of the old landslide. In case of heavy rain or long-term rainfall, this old landslide may be resurrected, threatening the stability of the airport site. To examine the mechanism of the failure induced by wetting for this unsaturated loess landslide, loess specimens were taken from the field, followed by performing a series of laboratory tests, including triaxial shear tests at constant matric suctions and wetting tests at constant deviator stresses. The test results revealed that the wetting-induced deformations of the loess included volume and shear deformations, reflecting compression and shearing behaviour induced by wetting. The failure behaviour of the loess along a wetting path was dependent on the stress level and the loss degree of matric suction as well as the hydro-mechanical path, and could be well described by the linear form of the Mohr-Coulomb strength theory. On this basis, the threshold value of the stress level was identified, which could be used to judge whether the wetting-induced failure of the loess occurs. The threshold value of matric suction at failure was also identified to analyse the loss degree of matric suction from stable conditions to failure. The mechanism of the failure of the soil due to wetting revealed from the present study could interpret the rainfall-induced landslide in unsaturated loess.

Keywords Loess landslide · Failures · Matric suction · Wetting · Triaxial test

Introduction

In China, loess area is 6.31×10^5 km², which predominantly distributes in northwestern China, covering several provinces Xinjiang, Gansu, Ningxia, Shaanxi and Shanxi (Liu 1985). The loess is mainly composed of silts, and its formation primarily involves provenance, transportation and deposition (Zhang et al. 1987; Derbyshire et al. 1998). As a result of such genesis, the loess features remarkably open structure and collapsibility (Lin, 2008). Loess features high void ratios and well-developed vertical joints which facilitate water infiltration, and its structure is affected by the cementation and arrangement of particles in sediment composition. With regard to collapsibility, the loess shows high shear strength and stiffness under natural conditions, which is significantly weakened once wetted, even while still being unsaturated (Gao 1988; Lin and Wang 1988; Zhou et al. 2014). Because of these

properties, loess slopes are particularly susceptible to landslide risk. Previous studies have revealed that the triggered factors for loess landslides have both natural factors and human activities. The natural factors include earthquakes (Wang and Zhang 1999; Zhang and Wang 2007; Wang et al. 2014b), frozen-thawing (Wang and Luo 2010), river erosion (Zhang and Liu 2010; Wang et al. 2019a) and rainfall (Xu and Zhang 2010; Zhang et al. 2014, 2017; Chen et al. 2018). The human activities include loading (Wang et al. 2018, 2019b), excavation (Zhang et al. 2012; Wang et al. 2014a) and agricultural irrigation (Zhang et al. 2009, 2013; Xu et al. 2012, 2014). Among them, rainfall and irrigation emerge as the most important triggering factors of loess landslides. A good understanding of mechanism of rainfall or irrigation-induced loess slope failures is of local engineering concern.

Landslides can be triggered by wetting of soil at a shallow depth due to rainfall (Wang et al. 2005, 2010, 2017; Sorbino and Nicotera, 2013) or rising of the water table in deep soil because of irrigation (Zhang et al. 2013; Xu et al. 2014). Most previous investigations on the failure mechanisms were primarily conducted through consolidated-undrained shear tests, constant shear drained tests and ring shear tests under controlled strain rates on saturated soils (Lade 1993; Sasitharan et al. 1994; Zhu and Anderson 1998; Sassa et al. 2003; Chu et al. 2003; Take et al. 2004; Lourenço et al., 2006; Zhang et al. 2013; Fan et al. 2017). These studies investigate the roles of excess pore water pressure and the salinity in pore water in the development of shear strength of saturated soils, and shed light on understanding the static liquefaction behaviours that led to flow initiation. In fact, the soils encountered in engineering practice are mostly unsaturated, and the potential slip surface may lie above the water table. A reduction of matric suction in the soil results in a decrease in effective normal stress on the potential failure surface, in turn lowers the shear strength (Brand 1981). The wetting-induced failure mechanism for unsaturated soils should thus be modelled under constant total stress condition while the pore water pressure is increased from an initial negative value until failure occurs. Two questions arise. What are the necessary requirements for the initial stress level and the degree of increase in negative pore water pressure (or matric suction) if wetting-induced the unsaturated loess failure occurs? How to describe? Until recent some researchers attempted to simulate the failure stress path by reducing matric suction while maintaining the deviator or shear stress at constant, for the loosely compacted completely decomposed granite, the sandy soil, the expansive clay and the loess (Chen et al. 2004; Farooq et al. 2004; Zhan et al. 2014; Zhou et al. 2014; Zhao and Zhang 2014). However, experimental results are still limited regarding the failure behaviour of unsaturated soils along the wetting path, especially for the collapsible loess with strong soil-water interaction.

The contribution of matric suction on shear strength of unsaturated soils has been investigated by means of shear tests at constant matric suctions (Maatouk et al. 1995; Khalili and Khabbaz 1998; Wang et al. 2002; Chen et al. 2014) or wetting tests

at constant shear stresses (Chen et al. 2004; Farooq et al. 2004; Zhan et al. 2014; Zhou et al. 2014). The point to be addressed is whether the contribution of matric suction on shear strength of unsaturated soils is independent of hydro-mechanical path followed, that is wetting-shearing (i.e. first wetting and then shearing) or shearing-wetting (i.e. first shearing and then wetting). This point is of importance when describing shear strength behaviours of unsaturated soils. Zhan et al. (2014) showed that the contribution of matric suction on shear strength of an unsaturated expansive clay was independent of the hydro-mechanical path. However, there is little information on the response of the collapsible loess to different hydro-mechanical paths.

In this study, a large-scale old landslide in the construction of Lvliang Airport in Shanxi Province was selected as a case (Fig. 1). If subjected to heavy rain or long-term rainfall, large slippage may occur and thus cause the instability of the airport site. Multiple ways in the investigation were adopted to reveal the landslide features, such as field surveys, borehole, exploration well and 1:500 terrain mapping. Two types of laboratory tests were carried out to study the wetting-induced failure mechanism of the unsaturated loess and the effect of the hydro-mechanical path on the shear strength. The first type was a series of strain-controlled triaxial shear tests at constant suctions; the second was a series of wetting tests at applied constant deviator stresses. Based on the field surveys and the experimental data, the initiation mechanism of old loess landslide subjected to water infiltration was interpreted.

Study area and field investigation

Lvliang Airport is located approximately 20.5 km away from Lvliang city in Shanxi Province, China (Fig. 1a). This is a typical mountain airport, and its construction accompanied by hill flattening and gully filling. At an early stage of this project, a large loess landslide was discovered on the southwest side of the Lvliang Airport runway (Fig. 1b). Under the influences of flood cutting and tectonic movement, the area where the landslides occurred has the characteristics of typical ridges and hills (Fig. 1b), and the terrain was high in the east and low in the west on the whole (Fig. 1c). The landslide with a circle chair-shape had a width of about 186 m, a horizontal length of about 260 m (along line A-A' in Fig. 1c), and a height of about 84 m from the boundary to sliding surface. The ground surface area affected by the loess landslide was nearly $3.6 \times 10^4 \text{ m}^2$, which was about 30° in average slope. The lithology is relatively simple in this region, and its lithological profile of the site can be mainly divided into three units (Fig. 2): (1) The top layer was composed of upper Pleistocene aeolian Malan loess which was about 1 to 16 m in thickness; (2) The bedrocks were made up of lower Carboniferous mudstone with minor sandstone partings; (3) Overlying the bedrocks was Pleistocene aeolian Lishi loess with several palaeosol partings, which was about 5 to 32 m in thickness.

According to the topography features, this landslide presented a progressive retreat development, which consisted of three sub-blocks, i.e. B-III, B-II and B-I (Fig. 1c). The total volume of the B-III was estimated to be approximately $1.2 \times 10^6 \text{ m}^3$. The trailing edge of the B-III was close to the filling area of the airport runway. The leading edge was basically erect, where there was subsidence of about 10 to 20 m. The B-II had volumes of about $2.7 \times 10^5 \text{ m}^3$, and could also be divided into two blocks, i.e. B-II-1 and B-II-2

(Fig. 1c). The B-II-1 was about 180 m in average width and 110 m in horizontal length. The landslide scar was remarkable, where there was subsidence of about 15 to 20 m (Fig. 1b). There were many well-developed gullies with about 3 to 8 m in deep on the back wall of the B-II-1. The landslide platform was gentle, with an average width of 35 m and an average inclination of 10° . The rear part of the landslide body and the back wall of the landslide were exposed by exploration wells (e.g. EW5, EW6, EW9 and EW16 in Fig. 1c), and no obvious fissures were found. These features revealed that this block was currently in a stable state. The B-II-2 was about 92 m in average width and 46 m in horizontal length. The landslide scar was also obvious, where there was subsidence of about 2 to 4 m (Fig. 1b). Significant sliding scratch surfaces were found by the exploration well (e.g. EW13 in Fig. 3b), and part of the landslide front had collapsed during survey, suggesting that this block displayed creep movement.

The B-I was located in front of the B-II (Fig. 1c). This block had volumes of about $1.1 \times 10^5 \text{ m}^3$. It experienced significant sliding, and thus, the boundaries were relatively clear. Due to the erosion of rainwater, this block further divided into three blocks, i.e. B-I-1, B-I-2 and B-I-3, as shown in Fig. 1c. The blocks B-I-1 to B-I-3 were about 43 to 66 m in widths and 47 to 78 m in horizontal lengths, as well as about 18° to 53° in the average slopes. The landslide scars were obvious, with subsidence of about 2 to 5 m. The back walls of the landslide were exposed by exploration wells (e.g. EW3 and EW4 in Fig. 1c), and the clear cracks at the trailing edge of the landslides were found. Significant sliding scratch surfaces were found at a borehole BH2 (Fig. 3a), suspecting to be a sliding shear surface. This indicated that the B-I was currently in the fretting phase.

The survey region belongs to arid or semi-arid climate. The seasonal distribution of rainfall is very concentrated. Typically, the average annual precipitation measured was about 460 mm. Rainfall varies with rainy and dry season, and about 75% of the annual rainfall occurs in the rainy season between June and September (Fig. 4). The maximum rainfall occurs in August, accounting for about 26% of the annual rainfall. This concentrated rainfall created conditions for the old landslide resurrection. On the one hand, both the leading edge of the landslide and its sides were significantly affected by rainfall erosion, forming a high-steep free face. This resulted in a higher initial mobilised shear stress of soil mass near the slope toe. On the other hand, there were obvious fissures in the landslide body. The surface rainwater was poured along those fissures, which was likely to accelerate the landslide resurrection and thus threaten the airport runway. In order to analyse landslide risk and optimise slope stabilisation strategies, a clear understanding of mechanisms of wetting-induced failure of the loess was required.

Laboratory testing

Materials and specimen preparation

Preliminary exploration well and borehole data indicated that the potential slipping zones were basically in the Lishi loess Q_2^{aol} layer (Fig. 2). To investigate the mechanism of wetting-induced failure of the unsaturated loess, the intact Q_2 loess used in this laboratory study was taken by manual cutting from the slope of the B-I-2 to keep the natural structure of loess, considering its high fragility. High-quality undisturbed block samples ($0.15 \text{ m} \times 0.15 \text{ m} \times 0.15 \text{ m}$

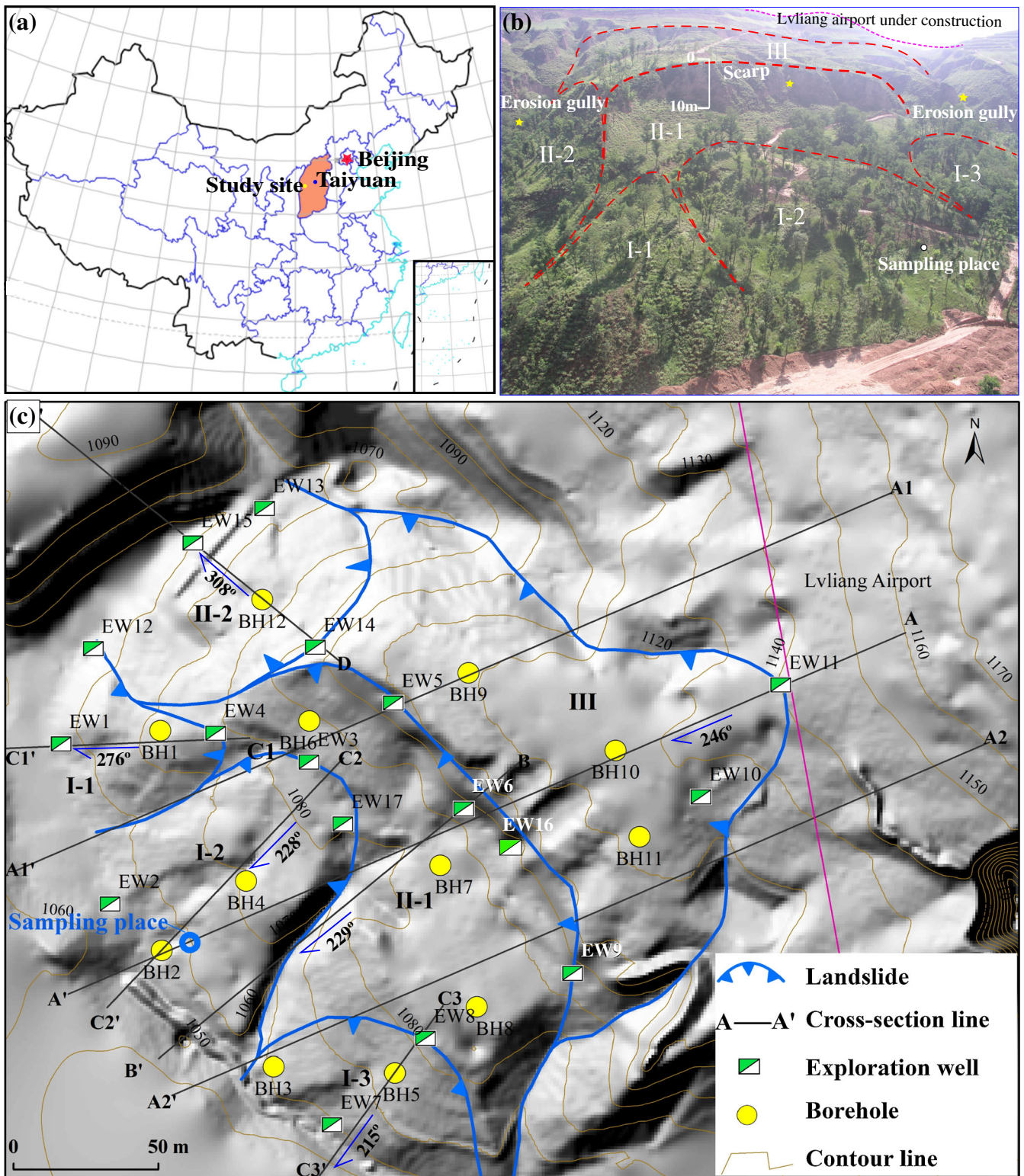


Fig. 1 a Location of study site; b a wide view of the loess landslide at Lvliang airport; c plan view and location of the landslide

in size) were collected at a depth of about 5 m. The block samples were protected by plastic membrane and waxed clothes, for preserving the in situ water content and soil structure. To prevent disturbance during cutting, the preparation of an intact block sample first involved cutting a small soil block with an appropriate

size. The ends of the specimen were trimmed with a wire saw, and then carefully trimmed to be a triaxial specimen, with diameter of 39.1 mm and height of 80 mm, using a special cutting apparatus. The difference in the dry density among the prepared intact specimens was not greater than 0.02 g/cm³. After completing the

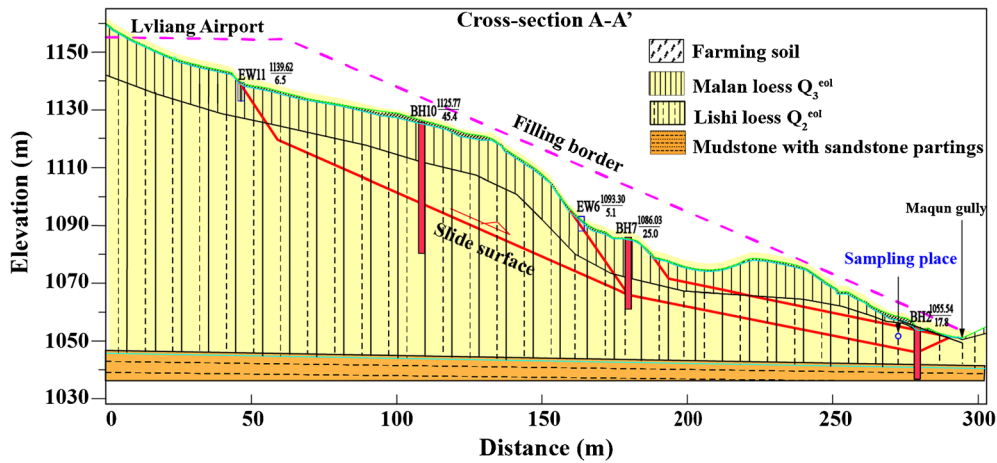


Fig. 2 Longitudinal section of the landslide along line A–A' in Fig. 1c

specimen preparation, the initial matric suction values of the intact specimens determined were 200 kPa via the null-type axis translation technique. The loess consisted mainly of silt (about 95%, Fig. 5) with some clay (about 14%). The mean particle diameter was 0.02 mm. The main physical indices of the intact loess taken from the field are illustrated in Table 1.

Apparatus

The unsaturated triaxial apparatus has been widely used to investigate the shear strength of unsaturated soils (e.g. Maatouk et al. 1995; Khalili and Khabbaz 1998; Wang et al. 2002; Chen et al. 2014). The unsaturated triaxial apparatus employed in the present research was modified by adding two devices, i.e. wetting device and stress-controlled loading device. Fig. 6 presents a schematic of this apparatus. The overview of the apparatus is shown in Fig. 6a. The wetting-induced shear mode of a specimen in the triaxial apparatus is shown conceptually in Fig. 6b. The wetting device was mainly a twin-tube with a different pressure transducer (Fig. 6a). When the valve was opened to link between the twin-tube and the perforated holes in the top cap, the water within the twin-tube was added gradually into the specimen (Fig. 6c). The change in water level within the twin-tube was measured by a different pressure transducer (range 6 kPa, precision 0.01 kPa), and then converted

to change in water volume (range 20 cm³, precision was 0.01 cm³). The stress-controlled loading device mainly consisted of a pneumatic actuator. The magnitude of the applied load and the axial deformation were recorded by a load transducer (range 5 kN, precision 1 N) and a displacement transducer (range 50 mm, precision 0.01 mm), respectively.

In addition, the axis translation technique (Hilf 1956) was employed to control or measure of matric suction in the specimen, using a 5-bar (i.e. 500 kPa) high-air entry ceramic disk. The overall volume change of the specimen was measured by monitoring the flow of water into the inner triaxial cell, similar to that employed by Wheeler (1988). Compression of the specimen resulted in a flow of water into the inter triaxial cell, which was measured with a volume change tube. The change in water level within the tube was monitored by a different pressure transducer, and then converted to change in water volume (range 40 cm³, precision was 0.01 cm³). Furthermore, the overall volume change was calibrated to eliminate the effects of confining pressure and loading ram displacement. This apparatus enabled the simulation of different stress paths tests for unsaturated soils, including wetting tests at constant stresses and shear tests at constant matric suctions. Further details about this apparatus can be found in Chen et al. (2017).

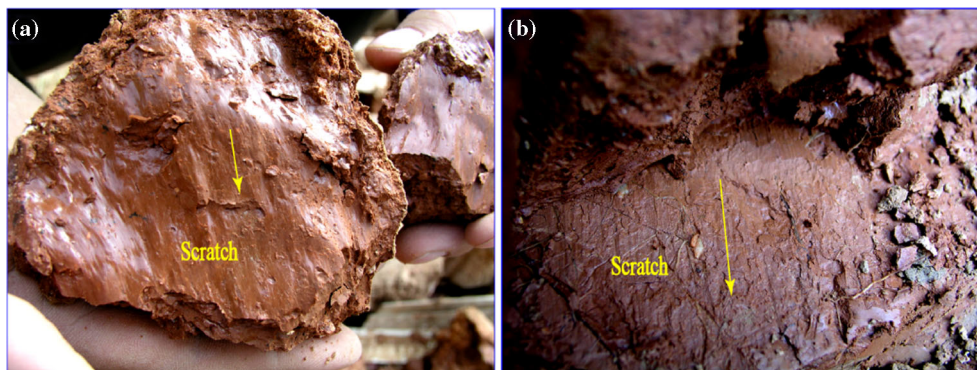


Fig. 3 Photos showing sliding scratch surfaces from different locations borehole (BH) or exploration well (EW) in Fig. 1c. a BH2; b EW13

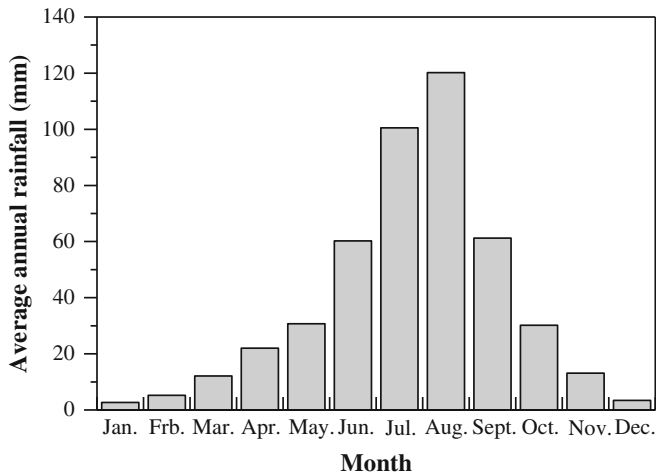


Fig. 4 The monthly distribution of the average annual rainfall applied in Lvliang Airport

Testing program and procedure

Two groups of laboratory tests were carried out to investigate the wetting-induced failure mechanism of the intact loess and the effect of the hydro-mechanical path on the shear strength, as summarised in Tables 2 and 3. Besides the principal stresses, the mean total stress is defined as $p = (\sigma_1 + 2\sigma_3)/3$ for axisymmetric condition ($\sigma_2 = \sigma_3$), $p - u_a$ is net mean stress, $q = \sigma_1 - \sigma_3$ is deviatoric stress, and $s = u_a - u_w$ is matric suction, where u_a and u_w are pore air and water pressures, respectively.

The first group of tests were shear tests (ST) involved conventional drained triaxial shear at constant matric suctions, i.e. the shear stages were carried out along a loading path of $q/(p - u_a) = 3$. The test results were to study the effects of matric suction and hydro-mechanical path on shear strength behaviours of the loess. Table 2 describes eight triaxial shear tests performed under controlled matric suctions and constant net confining pressures. The values of void ratio and degree of saturation after the isotropic

consolidation and the end of the test were given. The degree of saturation is calculated by combining change in overall volume and water volume of the specimen. Four net confining pressure values (50, 100, 200 and 400 kPa) and two matric suction values (0 and 200 kPa) were generally applied. The matric suction values chosen were to simulate the natural and saturated state of the loess, respectively.

For the ST, the σ_3 and u_a were both increased from zero to designed values during the isotropic consolidation. A stabilisation period was allowed until the increments in the overall volume and water volume were less than 0.01 cm^3 over an interval of 2 h. Following the isotropic consolidation, the conventional triaxial shear was performed at a strain rate of 0.004 mm/min under constant σ_3 and s .

The second groups of tests were wetting tests (WT) involved gradually increasing in pore water pressure from the negative value under constant total stress condition, i.e. decreasing matric suction from an initial value. The tests were to simulate the stress path of a slope element subjected to rainfall infiltration, whereby investigating wetting-induced the unsaturated loess failure behaviours. Table 3 describes 12 wetting tests performed under constant net confining pressures and stress levels, where stress level R_s is defined herein as the ratio of the current deviator stress q and the deviator stress at failure q_f , i.e. $R_s = q/q_f$. The values of void ratio and degree of saturation after the triaxial shear and the end of the test were given. Four net confining pressure values (50, 100, 200 and 400 kPa) and three stress level values (0.25, 0.50 and 0.75) were generally applied. The stress level values were chosen to simulate the stress state of the soil mass at different locations on the loess slope.

For the WT, each natural specimen was loaded at a suction of 200 kPa to different target σ_3 and R_s along the same stress path as the ST. Following this stage, the specimen was wetted from natural matric suction by adding precalculated volumes of water in steps at constant σ_3 and R_s . The wetting criterion was proposed, i.e. the wetting series was at least six or the water content increment was no less than 2%. For each step wetting, the pore air pressure u_a of 200 kPa maintained constant. The air backpressure slightly larger

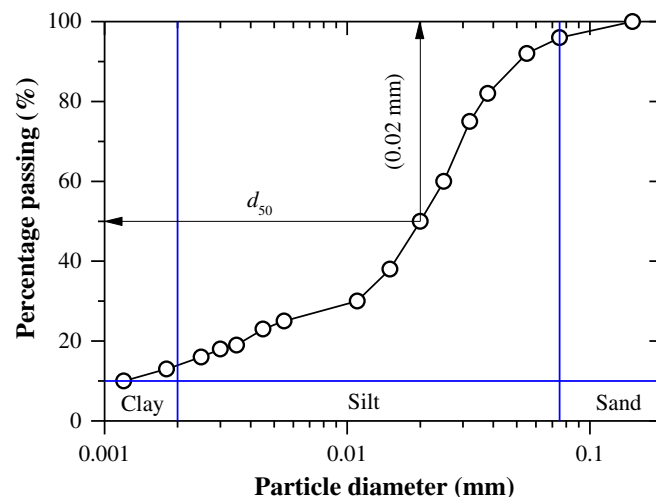


Fig. 5 Particle-size distribution of Lishi loess

Table 1 Physical properties of soil specimens

Sample	w (%)	G_s	ρ (g/cm ³)	ρ_d (g/cm ³)	e	w_L (%)	w_p (%)	I_p (%)	Classification
Lishi loess	14.0	2.70	1.69	1.48	0.82	26.4	14.9	11.5	Silty clay

w water content, G_s specific gravity of soil grain, ρ natural density, ρ_d natural dry density, e void ratio, w_L liquid limit, w_p plastic limit, I_p plasticity index

than the u_a was applied to the wetting twin-tube, and then the valve was opened at a tiny angle of about 10° , for linking the twin-tube and the top cap. The tiny angle was to avoid local failure in the top of the specimen. The water within the twin-tube was added to the specimen gradually. As the amount of water reached the water volume corresponding to the target water content increment, the valve was closed. The variations of overall volume change, axial deformation and pore water pressure over time were live recorded. A stabilisation period was allowed until the overall volume change increment was less than $0.01 \text{ cm}^3(2 \text{ h})^{-1}$, the axial deformation increment was less than 0.005 mm h^{-1} and the suction increments were less than $1 \text{ kPa}(2 \text{ h})^{-1}$.

Test results

ST results

In this section, the effects of the matric suction and the net confining pressure would be described. Under $\sigma_3 - u_a = 50$ and

200 kPa, the variations of deviator stress, volumetric strain and degree of saturation with axial strain at various matric suctions (from 200 to 0 kPa) are presented in Fig. 7. All curves were well ordered and evolved regularly with decreasing matric suction. There were no peaks in the stress-strain curves, illustrating a lower brittleness and reaching the critical state at larger strains. The initial modulus and deviator stress decreased with matric suction. The volumetric contraction induced by shearing was observed, and the volumetric strain became large with decreasing in the matric suction. This indicates that the loess specimens undergo strain hardening behaviour during shearing, and the extent of which is dependent on matric suction. Furthermore, the degree of saturation of the specimen increased during shearing at matric suction of 200 kPa, which was the results of both water absorption and contraction of the specimen.

The effect of the net confining pressure is illustrated in Fig. 8, where all test results at matric suctions of 200 and 0 kPa are plotted together, respectively. As usual, under $s = 0$ kPa, the deviator stress and initial

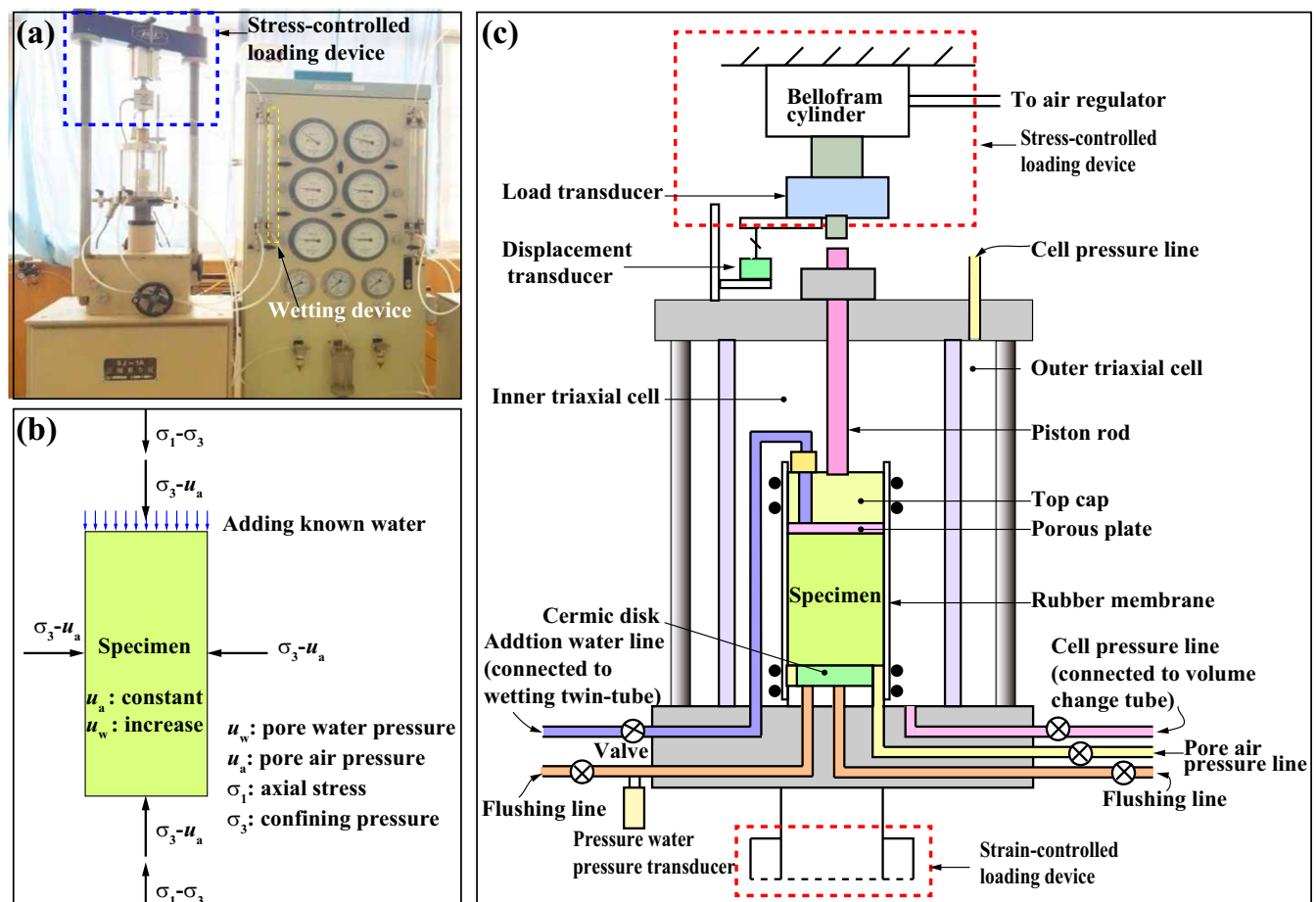


Fig. 6 Suction-monitored triaxial apparatus. a Overview; b specimen in triaxial cell; c schematic diagram of suction-monitored triaxial apparatus

Table 2 Testing program and result summary of the ST tests

Group	Test	s (kPa)	$\sigma_3 - u_a$ (kPa)	After isotropic consolidation but prior to shear		Critical state when test is terminated				
				e	S_r (%)	e_f	S_{rf} (%)	q_f (kPa)	c (kPa)	ϕ (°)
ST1	ST1-1	200	50	0.82	46.1	0.76	52.1	335	61	29
	ST1-2	200	100	0.82	46.4	0.71	55.1	389		
	ST1-3	200	200	0.81	45.6	0.69	55.9	625		
	ST1-4	200	400	0.79	45.3	0.66	55.4	825		
ST2	ST2-1	0	50	0.82	100	0.73	100	48	0	29
	ST2-2	0	100	0.80	100	0.66	100	231		
	ST2-3	0	200	0.79	100	0.63	100	388		
	ST2-4	0	400	0.78	100	0.61	100	755		

s matric suction, σ_3 confining pressure, u_a pore air pressure, S_r degree of saturation

modulus increased with the net confining pressure. For $s = 200$ kPa, at strains larger than 3% the deviatoric stress increased with the net confining pressure, whereas the change in initial modulus was not obvious. This possible reason may be related to the initial structural of the loess. All volume change curves show an increase of compressive behaviour with net confining pressure, suggesting that the effect of the net confining pressure is clear. In addition, the degree of saturation of the specimen at matric suction of 200 kPa increased with axial strain. The observation concerning the slight influence of the net confining pressure on the degree of saturation was valid for $(\sigma_3 - u_a) > 50$ kPa.

As commented above, intact specimens from in situ sites show a contractive and ductile behaviour, i.e. the stress-strain curves show hardening. At axial strains of 15%, assuming all specimens reach a critical state, similar to that employed by Oka et al. (2010) and Chen et al. (2014). The critical state from ST at matric suctions of 200 and 0 kPa are shown on a $q - p$ plane in Fig. 9a, and the corresponding shear strength q_f are presented in Table 2. At a given matric suction, the critical state line (CSL) was well fitted to a straight line on the $q - p$

plane, suggesting that the shear strength of the loess can be described by the Mohr-Coulomb strength criterion. The CSL at unsaturated and saturated states were approximately parallel, and slopes of which M were 1.167. Furthermore, the cohesion c and internal friction angle ϕ of the loess at the saturated and unsaturated states were determined by formulas, i.e. $c = (3 - \sin\phi)/(6\cos\phi) h$ and $\phi = \sin^{-1}[3M/(6 + M)]$, where h is the intercept of the critical state line, its values are shown in Table 2. The internal friction angles hold constant, whereas the cohesion c decreased with matric suction. The above results indicate that the shear strength of the loess is strongly sensitive to the matric suction, and the matric suction-dependency of shear strength behaviour is reflected primarily by focusing on the evolution of the cohesion (so-called “bonding effect”). This observation suggests that the bonding effect plays a major role in the triggering phenomena of the loess landslides investigated.

To further analyse the shear strength of the loess, the skeletal stress p' , or referred to as “effective mean stress”, was chosen, i.e. $p' = p + S_r s$ (Gallipoli et al. 2003; Nuth and Laloui 2008). The above

Table 3 Testing program and result summary of the WT tests

Group	Test	s_0 (kPa)	$\sigma_3 - u_a$ (kPa)	R_s	After shear but prior to wetting		Critical state/final state when test is terminated		
					e	S_r (%)	s_f	e_f	S_{rf} (%)
WT1	WT1-1	200	50	0.25	0.82	46.3	/	0.75	99.5
	WT1-2	200	50	0.50	0.81	46.7	12	0.73	95.0
	WT1-3	200	50	0.75	0.79	46.8	57	0.66	88.0
WT2	WT2-1	200	100	0.25	0.81	46.5	/	0.71	99.1
	WT2-2	200	100	0.50	0.81	46.9	25	0.68	91.0
	WT2-3	200	100	0.75	0.78	48.6	81	0.68	75.0
WT3	WT3-1	200	200	0.25	0.81	46.8	/	0.69	99.3
	WT3-2	200	200	0.50	0.78	48.8	26	0.67	95.0
	WT3-3	200	200	0.75	0.74	51.4	117	0.67	66.0
WT4	WT4-1	200	400	0.25	0.78	48.7	/	0.65	99.7
	WT4-2	200	400	0.50	0.76	49.9	/	0.63	99.7
	WT4-3	200	400	0.75	0.72	52.8	65	0.67	87.5

s_0 initial matric suction, R_s stress level, / no failure during wetting, s_f matric suction when failure due to wetting

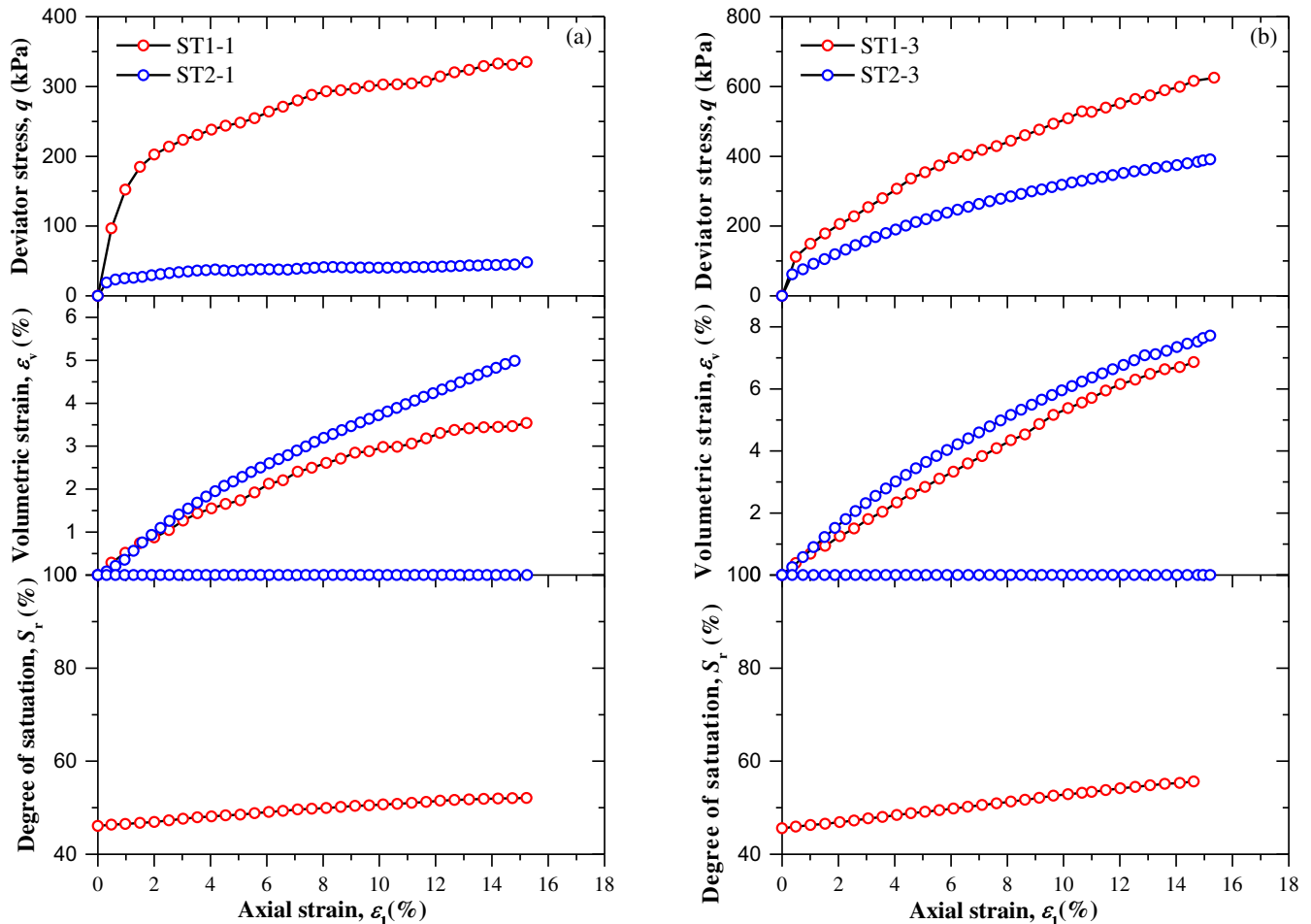


Fig. 7 Effect of matric suction on the stress-axial strain, volumetric strain-axial strain and degree of saturation-axial strain curves for various controlled net confining pressures. a $\sigma_3 - u_a = 50$ kPa; b $\sigma_3 - u_a = 200$ kPa

results are expressed on a $q - p'$ plane as shown in Fig. 9b. For each test, the value of the deviatoric stress q at critical state is reported as a function of the value of the effective mean stress p' . The experimental data appear to confirm the existence of a unique failure envelope for the loess, if the adopted stress variables take into account both matric suction and degree of saturation; moreover, this envelope is well described by the same line adopted for representing the critical state of the saturated soil.

WT results

The deviator stress, matric suction, axial strain and volumetric strain relationships from the WT are presented in Fig. 10. The deviator stress-axial strain curves from the ST, at a constant matric suction of 200 kPa but various net confining pressures, are also shown for comparison. At a given deviator stress, the matric suction was decreased gradually from initial value of 200 kPa during wetting, causing increase in both volumetric strain and axial strain, monotonously. This indicates that the wetting-induced deformation of the loess consists of two components: wetting-induced volume and shear deformations, reflecting compression and shearing behaviour of the loess induced by wetting, respectively. For a given net confining pressure, the axial strain and volumetric strain during wetting increased with the stress

level, but the difference in increasing rates were observed. At a low stress level, the increasing rate of the volumetric strain during wetting was larger than that of the axial strain, such as WT1-1 and WT4-1, suggesting that the compression behaviour of the loess induced by wetting dominates. At a high stress level, this behaviour followed the opposite trend, such as WT1-3 and WT4-3, indicating that the shearing behaviour of the loess induced by wetting dominates. In addition, for a given stress level, as the net confining pressure increased, the wetting-induced axial strain exhibited increase firstly and followed by decrease, suggesting that the net confining stress appeared to restrain the shearing behaviour of the loess induced by wetting.

Figure 10 also revealed that once matric suction in the specimen was reduced to the certain value, the development of axial strain accelerated with the additional decrease in matric suction, while the volumetric strain remained basically unchanged, appearing the tendency for the wetting-induced the specimen failure, such as WT1-2, WT1-3, WT2-2, WT2-3, WT3-2, WT3-3 and WT4-3. At axial strains of 15%, assuming the specimen subjected to wetting reaches a critical state. The matric suction s_f at failure has been marked in Fig. 10, and value of that presented in Table 3. As expected, the value of matric suction at failure increased with the stress level, and increased firstly and then decreased with increase in the net

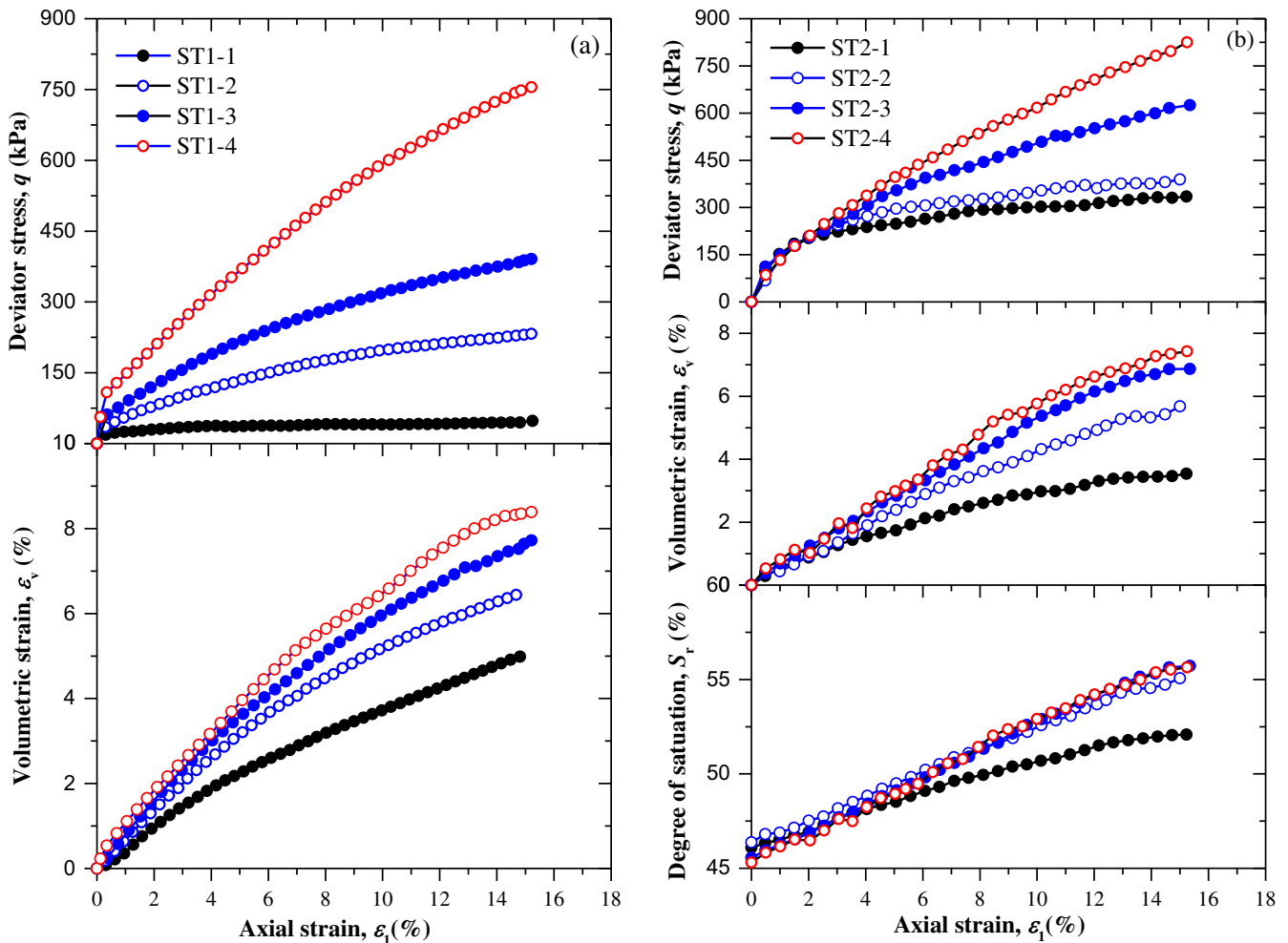


Fig. 8 Effect of net confining pressures on the stress-axial strain, volumetric strain-axial strain and degree of saturation-axial strain curves for various controlled matrix suctions. a $s = 0$ kPa; b $s = 200$ kPa

confining pressure. In other words, the wetting-induced the loess failure behaviour is dependent on the stress level, net confining pressure and matric suction.

The soil water characteristic curves (i.e. SWCCs) of the loess are presented in Fig. 11 by means of the data presented above (Fig. 10). The degree of saturation S_r exhibited a rapid increase firstly and followed by a slight change, as the matric suction s decreased. The

SWCC moved to the upper right with an increase in the stress level, suggesting stress-dependency SWCCs of the loess. Essentially, the stress level not only causes a change in the soil density (or void ratio) and thus its saturation (Table 3), but also results in the variation of pore size distribution (Zhou et al. 2014), similar to the observation reported by Romero et al. (2011). The features of the SWCC can be used to describe the variation of shear strength in the soil with matric suction.

The WT results (Figs. 10 and 11) are plotted on the $q - p'$ plane, as shown in Fig. 12. The CSL determined by ST (Fig. 9b) are also shown for comparison. The specimen was subjected to wetting from natural state along a $q = \text{constant}$ path (marked by symbol 'o'), causing the decrease in the matric suction and thus the reduction in the effective mean stress (marked by an arrow). Some specimens wetted to matric suction s_f were observed to fail (marked by symbol '●'), suggesting that the process of the wetting-induced failure for the unsaturated loess can be visually described on the $q - p'$ plane; meanwhile, all data points corresponding to the failure appeared to lie on a straight line through the origin with a slope M_s of 1.022. This indicates that the wetting-induced the loess failure behaviour could be described by the linear form of the Mohr-Coulomb strength theory. Moreover,

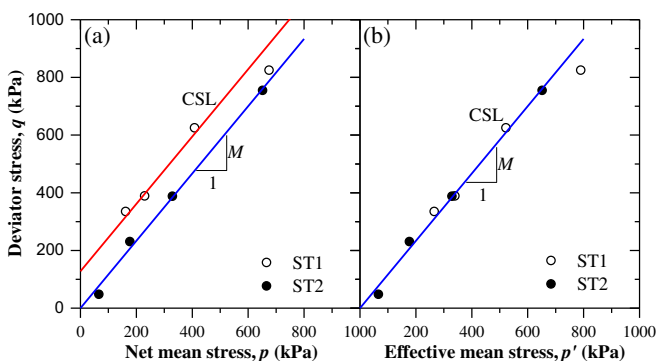


Fig. 9 Critical state lines on $q-p$ and $q-p'$ planes from ST results

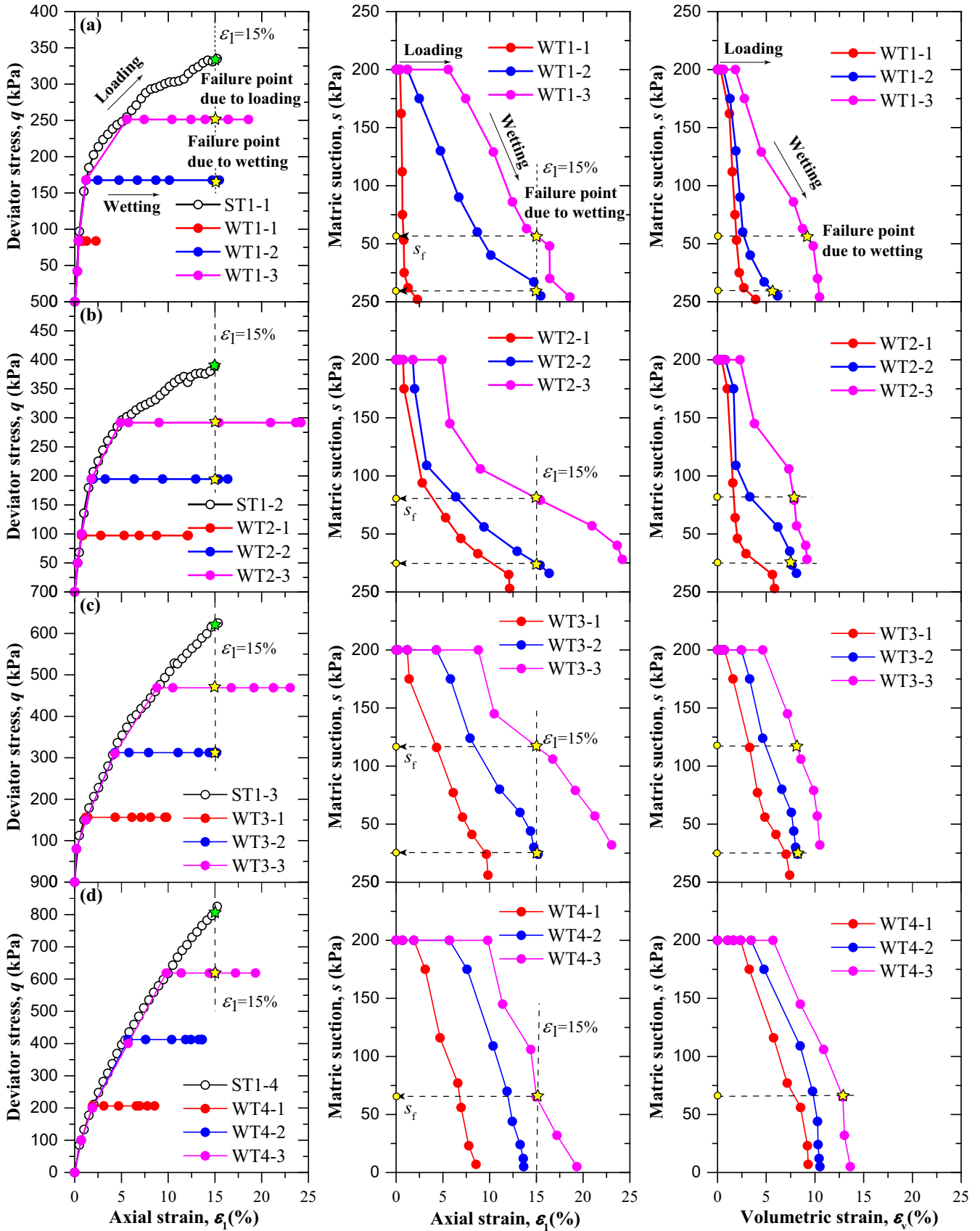


Fig. 10 Deviator stress-axial strain, matric suction-axial strain and matric suction-volumetric strain curves from WT at various controlled net confining pressures. **a** $\sigma_3 - u_a = 50$ kPa; **b** $\sigma_3 - u_a = 100$ kPa; **c** $\sigma_3 - u_a = 200$ kPa; **d** $\sigma_3 - u_a = 400$ kPa

The CSL determined by the WT was below that determined by the ST, revealing that the contribution of matric suction on shear strength of the loess is dependent on the hydro-mechanical path. Based on the shear tests at constant matric suctions, the variations in shear strength parameters (i.e. c and ϕ) with matrix suction were obtained to describe the wetting-induced the loess failure behaviour, which was unsafe for engineering applications.

The test results for the specimens wetted to near saturation without failure are also plotted on the $q - p'$ plane, as shown in Fig. 16 (marked by symbol '●'). Interestingly, for the lower of the stress level, the phenomenon of no failure occurred when wetted from natural state to near saturation (e.g. WT3-1); for the higher of the stress level, the phenomenon of failure occurred when wetted from natural state to the different levels of matric suction (e.g. WT3-2 and WT3-3). Therefore, it could be inferred that there is a threshold value of stress level R_{sr} at which the phenomenon of failure will just occur when wetted from natural state to saturation. A simplified diagram was plotted to determine the threshold value of stress level R_{sr} (Fig. 13). Point A (p_1', q_1') was the current stress state of the specimen at natural matric suction s_0 , and the corresponding shear strength and stress level were represented by q_f and $R_s (= q_f/q_1')$. The failure occurred when the specimen was wetted to saturation at constant deviator stress, and the corresponding stress state shifted from point A (p_1', q_1') to point B (p_2', q_1') on the critical state line. The stress level R_s thus was the threshold value of stress level R_{sr} . Assuming the value of matric suction was 0 kPa at saturation, the effective mean stress increment $\Delta p'$ from point A to point B was

$$\Delta p' = p_1' - p_2' = p S_{ro} s_0 \quad (1)$$

where S_{ro} is the degree of saturation before wetting. In addition, the effective mean stresses p_1' and p_2' can be rewritten as

$$p_1' = \frac{q_f}{M}, p_2' = \frac{q_f}{M_s} = \frac{q_f R_{sr}}{M_s} \quad (2)$$

The threshold value of stress level R_{sr} can be obtained via Eq. (2) and Eq. (1)

$$R_{sr} = \frac{q_f/M - \Delta p'}{q_f/M_s} \quad (3)$$

A reduction factor $\xi (= M_s/M)$ is introduced, and thus Eq. (3) can be rewritten as

$$R_{sr} = \xi \left(1 - \frac{M \Delta p'}{q_f} \right) = \xi \left(1 - \frac{\Delta p'}{p'} \right) = \xi \left(1 - \frac{S_{ro} s_0}{p + S_{ro} s_0} \right) \quad (4)$$

According to Eq. (4), the higher the p , the higher is the R_{sr} , and vice versa. This was related to the loading hardening of the loess before wetting. If wetting-induced the loess failure occurs, the initial deviator stress level R_s must meet the following criterion:

$$R_s \geq R_{sr} = \xi \left(1 - \frac{S_{ro} s_0}{p + S_{ro} s_0} \right) \quad (5)$$

For the loess studied, the values of ξ and s_0 are equal to 0.876 and 200 kPa, and values of S_{ro} before wetting are shown in Table 2. Using Eq. (5), the threshold line of potential failure due to wetting can be determined on the $q - p'$ plane, as shown in Fig. 12. It was clearly observed that the threshold line could well judge whether the wetting-induced the loess failure occurred. If the stress state before wetting was above the threshold line, the wetting-induced failure may occur; otherwise, wetting-induced failure was unlikely to occur. The threshold value of stress level may be an important control parameter in the early warning system for rainfall-induced landslides in unsaturated loess.

For $R_r \geq R_{sr}$, if the wetting-induced failure occurs, the loss degree of matric suction Δs must meet the following criterion:

$$\Delta s \geq (s_0 - s_f) \quad (6)$$

The threshold value of the matric suction s_f has practical engineering significance, for controlling the loss degree of matric suction from stable conditions. A simplified diagram was also plotted to determine the threshold value of matric suction s_f at failure, as shown in Fig. 13. The failure occurred when the specimen was wetted to the matric suction s_f at constant deviator stress $q (\geq q_r$, i.e. $R_r \geq R_{sr}$), and the corresponding stress state shifted from point E to point F on the critical state line (Fig. 13). The effective mean stress increment $\Delta p'$ was

$$\Delta p' = p(S_{ro} s_0 - S_{rf} s_f) \quad (7)$$

where S_{rf} is the degree of saturation corresponding to the matric suction s_f . Similar to the above derivation, the R_s was substituted for R_{sr} in Eq. (4), and substituting Eq. (7) into Eq. (4) leads to:

$$R_s = \xi \left(1 - \frac{S_{ro} s_0 - S_{rf} s_f}{p + S_{ro} s_0} \right) \quad (8)$$

Eq. (8) can be rewritten as

$$S_{rf} s_f = S_{ro} s_0 - (1 - R_s / \xi) (p + S_{ro} s_0) \quad (9)$$

The suction stress $S_r s$ is plotted against matric suction s in Fig. 14 by means of the data presented above (Fig. 11). The $S_r s$ decreased with the s . The data for different stress states appeared to lie on a curve, which could be represented by an empirical formula below:

$$S_r s = \frac{s}{\alpha s + \beta} \quad (10)$$

where α and β are soil parameters. Regression of the data to this formula resulted in $\alpha = 0.005 \text{ kPa}^{-1}$ and $\beta = 1.020$. Equations (9) and (10) are the quantitative relationship between the stress level $R_s (\geq R_{sr})$ and the matric suction s_f at failure. It can clearly be seen that the larger the R_s , the larger is the s_f , and vice versa. In addition, when $R_s = \xi$ the s_f is equal to the s_0 , suggesting that failure occur once the specimen is wetted at critical state line determined by WT; when $R_s = R_{sr}$ the s_f is equal to zero, i.e. Eq. (9) degenerates into Eq. (5). Using Eqs. (9) and (10), the results of $R_s - s_f$ and $q - s_f$ relations were predicted, and the typical results of

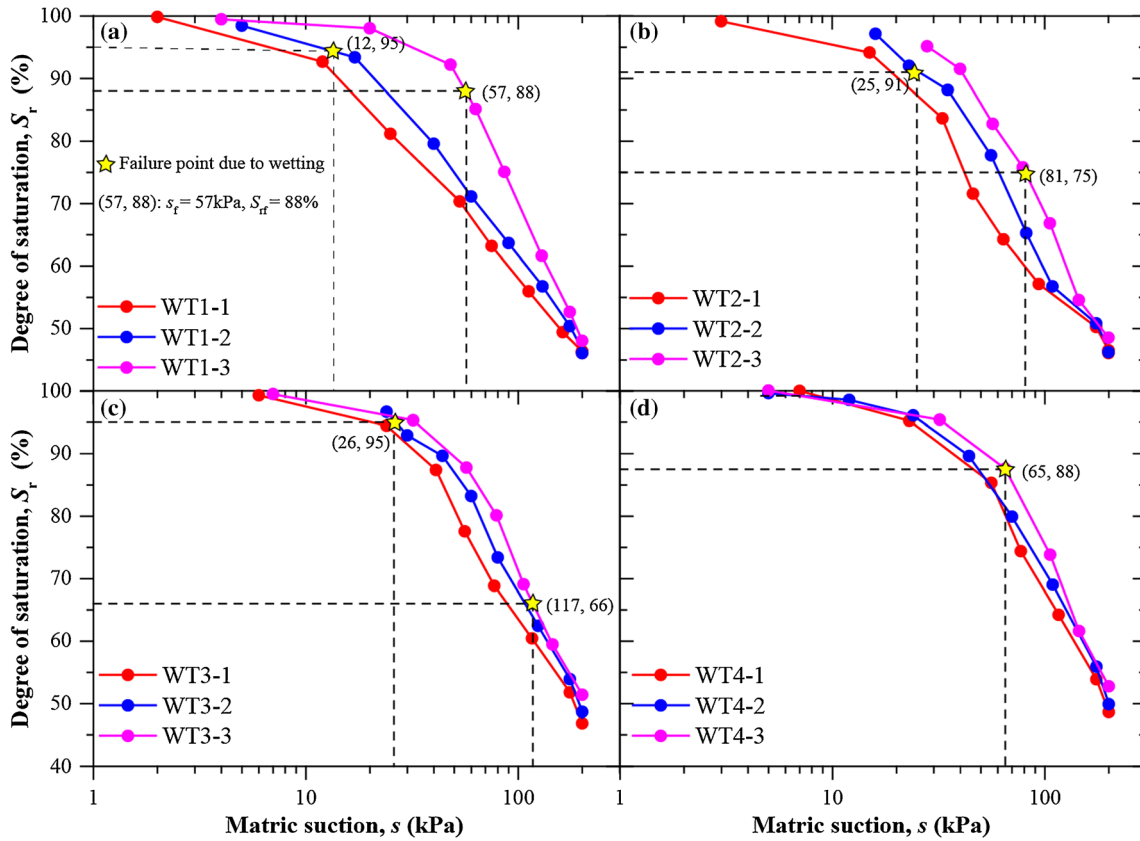


Fig. 11 Soil-water characteristic curves from WT at various controlled net confining pressures. **a** $\sigma_3 - u_a = 50$ kPa; **b** $\sigma_3 - u_a = 100$ kPa; **c** $\sigma_3 - u_a = 200$ kPa; **d** $\sigma_3 - u_a = 400$ kPa

the predictions together with the corresponding experimental data are shown in Fig. 15a, b. The prediction results quite close to the experimental results.

Discussion

Based on the above field surveys and experimental results, the observed failure process of the unsaturated loess slope (Fig. 1) was interpreted further as follows. The area where the landslides

occurred is characterised by ridges and hills (Fig. 1). These structures are bound by steep slopes with high-free faces, resulting in the stress concentration at the foot of the slope. This creates favourable condition for the occurrence of the loess landslide. The schematic representation of the loess slope at the natural state is shown in Fig. 16a. Points A, B, C and D, which represent the initial stress state of different positions in the slope, have to be below the CSL in a $q-p'$ diagram (Fig. 16a-1).

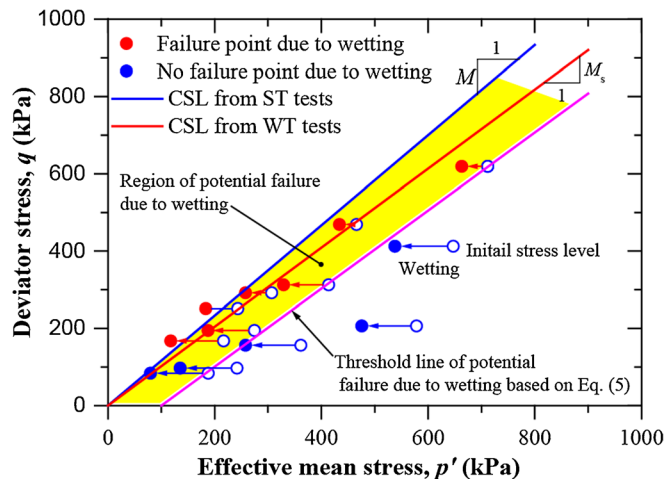


Fig. 12 Critical state lines on $q-p'$ planes from WT

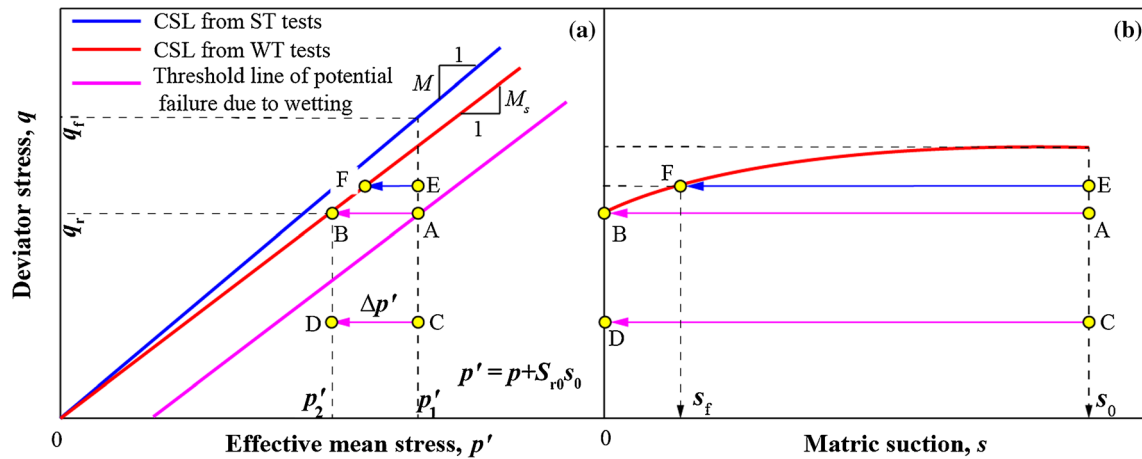


Fig. 13 A simplified diagram for determining the threshold values of stress level R_{sr} and matric suction s_f at failure

Due to the concentrated rainfall in the area (Fig. 4), the rainfall-induced floods often occur. The lateral erosion and downward erosion of the flood caused both sides of the gully to collapse continuously, in turn widening and deepening the gully (e.g. Maqun gully in Fig. 1). This promoted the redistribution of the stress inside the slope, and its effect was reflected in two aspects. On the one hand, the free face of the leading edge of the slope became steep, so that its resistance of the leading edge was reduced, and a strong shear stress region was formed at the bottom of the slope (Fig. 16b). On the other hand, the lateral support to upper soil masses would be lost, producing horizontal deformation of the soil mass towards the free face (Fig. 16b). Consequently, the strong tensile zone was formed at the top of the slope. This process was similar to that the vertical stress (i.e. larger principal stress) hold constant, while the lateral stress (i.e. small principal stress) decreased. For different positions in the slope, the effective stress paths in the q - p' plane followed by the stress state in Fig. 16b-1. With further increase in the horizontal deformation, the small principal stress at the top of the slope would be reduced to a negative value, whereby the

tensile crack would appear, such as point A_1 in Fig. 16b. As the degree of erosion at the foot of the slope increased, a new region of tensile stress concentration would form at the bottom of the tensile crack, promoting the crack to enlarge and extend deep into the slope (Fig. 16c). Thereby, partial loss of support and release of side restraint could cause the locally failed part to move downslope, increasing the load there. In other words, the range of the shear stress region in soil mass was thus narrowed. The initial shear stress level of soil mass near the slope toe would be higher. More importantly, the generation of cracks provided a dominant channel, and water could infiltrate along these cracks directly and rapidly, accelerating the infiltration of surface rainwater into the deep slope. The stress path of the above process is shown in Fig. 16c-1. In a word, the erosion of floods accelerated the initiation of the landslide.

Due to constant climatic changes during the Quaternary, the hydraulic and mechanical properties of the silty loess from the Lishi loess layer have obvious differences compared to the palaeosol, which created the basic condition for the formation of weak sliding zone. The silty loess has a relatively high content of silt particle, and its soil layer is relatively loose and easy to water seepage. While the palaeosol has a high content of clay particle, and its soil layer is dense, playing a relatively impermeable role. When subjected to the rainfall, rainwater would enter the soil slope through the cracks, leading to an increase in the weight of the soil mass and thus the sliding force of the slope. On the other hand, the interface between the silty loess and the palaeosol layers formed a water-rich zone, causing a rapid decrease in matric suction of the upper silty loess mass. Corresponding to the in situ situation, the stress path of the slope was similar to wetting at a $q = \text{constant}$ (i.e. WT, Fig. 10). A reduction of suction resulted in a decrease of the effective mean stress of the upper silty loess mass, with a consequent swift reduction of shear resistance (Fig. 12). Whether the wetting-induced the silty loess failure would occur, which was dependent of both the stress level and the loss degree of matric suction (Fig. 12). According to the WT results, the threshold line of potential failure due to wetting could be determined using Eq. (5).

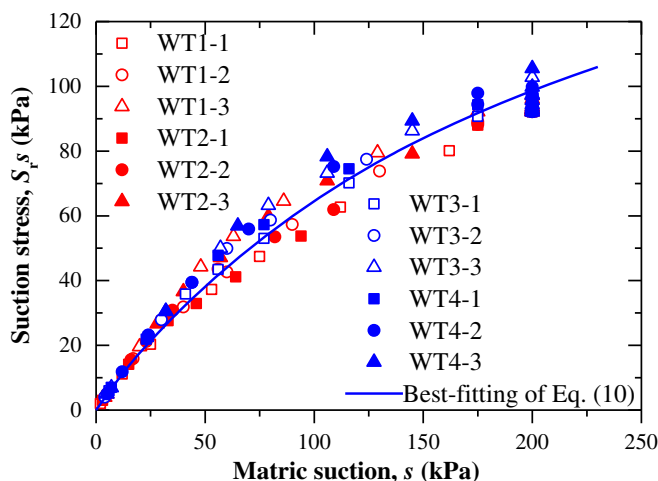


Fig. 14 Suction stress S_{rs} against matric suction s from WT

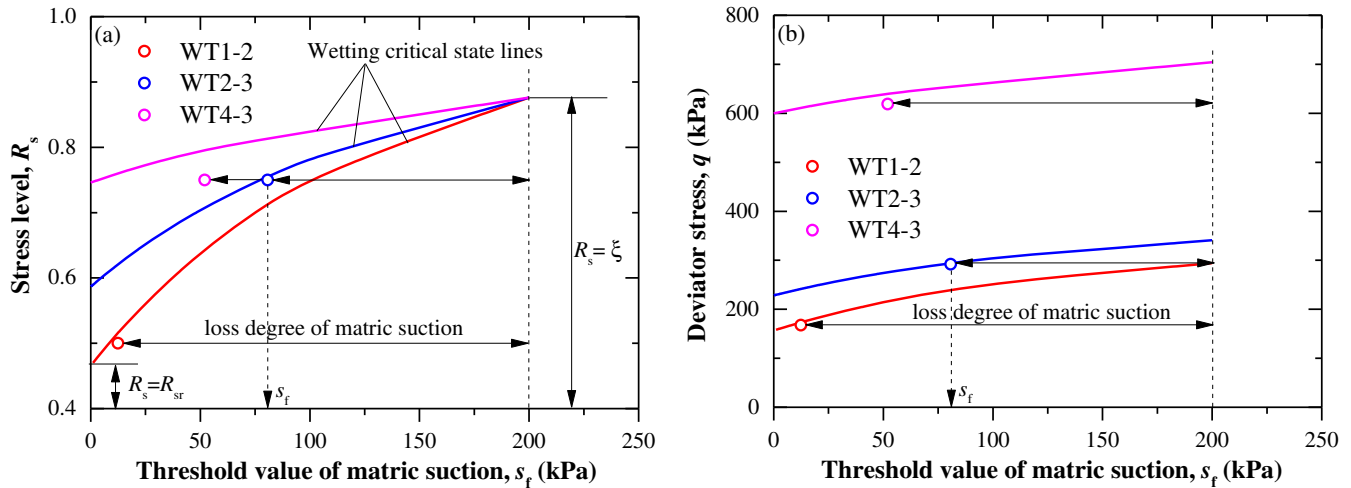


Fig. 15 Deviator stress level or deviator stress against matric suction from WT

Furthermore, the stress state of the soil slope was affected by the angle and height of the slope. Therefore, the relationship between the stress level corresponding to the threshold line and those factors may be established, in turn applying to judge preliminarily whether there is a risk of wetting-induced loess landslides. For the loess slope with a lower angle, the maximum value in stress level before wetting was below the threshold line, then the stress path along wetting to saturation at a $q = \text{constant}$ would not reach the CSL line. In other words, such a slope would be stable even when wetted to saturation.

For the loess slope with a higher angle, if the value in stress level before wetting was above the threshold line, the wetting-induced loess landslide may occur. Using the threshold line of potential failure, it may be possible to predetermine the approximate range of the potential slip zone induced by water infiltration (Fig. 16d). When the stress level before wetting such as point C_2 was below the threshold line (Fig. 16c-1), the failure would not occur even if the soil mass was wetted to saturation such as point C_3 (Fig. 16d-1). When the stress level before wetting such as point B_2 or D_2 was above the threshold line (Fig. 16c-1), the stress state along wetting at a $q = \text{constant}$ would likely move to the point such as point B_3 or D_3 on the CSL line (Fig. 16d-1). Whether the failure occurs was related to the loss degree of matric suction in soil mass induced by rainfall (Fig. 15). The higher the stress level, the lower was the loss degree of matric suction at failure (Fig. 15). This was reason that the humidifies of the sliding zone were different at various locations (Fig. 2). As a result, the continuous decrease in suction caused a significant reduction in shear strength of silty loess mass, which triggered a local failure in a slope. When the tension crack zone and the failure zone due to wetting connected gradually, and a continuous slide surface would be formed (Fig. 16d). After the occurrence of landslide, the steep back scarp would be formed on the trailing edge of the landslide, and the new tensile stress distribution area would also be formed (Fig. 16e). Repeating the above process, the loess landslide showed a progressive retreat development (Fig. 1).

Conclusions

In this study, multiple ways in the field surveys were adopted to reveal the loess landslide features in Lvliang Airport, China. Laboratory tests including triaxial shear tests at constant suctions (i.e. ST) and wetting tests at constant stresses (i.e. WT) were carried out, for investigating the wetting-induced failure mechanism of the loess and the effect of the hydro-mechanical path on the shear strength. The conclusions drawn are as follows.

Tendency of contraction was the volumetric behaviour of the loess following stress path of the ST. The critical state line (CSL) determined by ST was unique in the deviatoric stress-effective mean stress ($q - p'$) plane, for both saturated and unsaturated loess. The contribution of matric suction on shear strength of the loess was dependent on the hydro-mechanical path. The relationship between shear strength parameters obtained by ST and the matrix suction was used to describe the wetting-induced the loess failure behaviour, which was unsafe for engineering applications.

The wetting-induced deformation of the loess consisted of two components: wetting-induced volume and shear deformations, reflecting compression and shearing behaviour induced by wetting, respectively. At a low stress level, the wetting-induced compression behaviour dominated; otherwise, the wetting-induced shearing behaviour dominated. The wetting-induced the loess failure behaviour was strongly dependent on the stress level and the loss degree of matric suction, which could well be described by the linear form of the Mohr-Coulomb strength theory.

A threshold value of stress level was identified, i.e. the phenomenon of failure occurred when wetted to saturation at this value. It was dependent on the net mean stress and the initial matric suction, and could be well described by the proposed function (i.e. Eq. (5)). This value could be used to judge whether the wetting-induced the loess failure may occur, and thus may be an important control parameter in the early warning system for rainfall-induced landslides in the unsaturated loess. A threshold value of matric suction was identified to analyse the loss degree of matric suction from

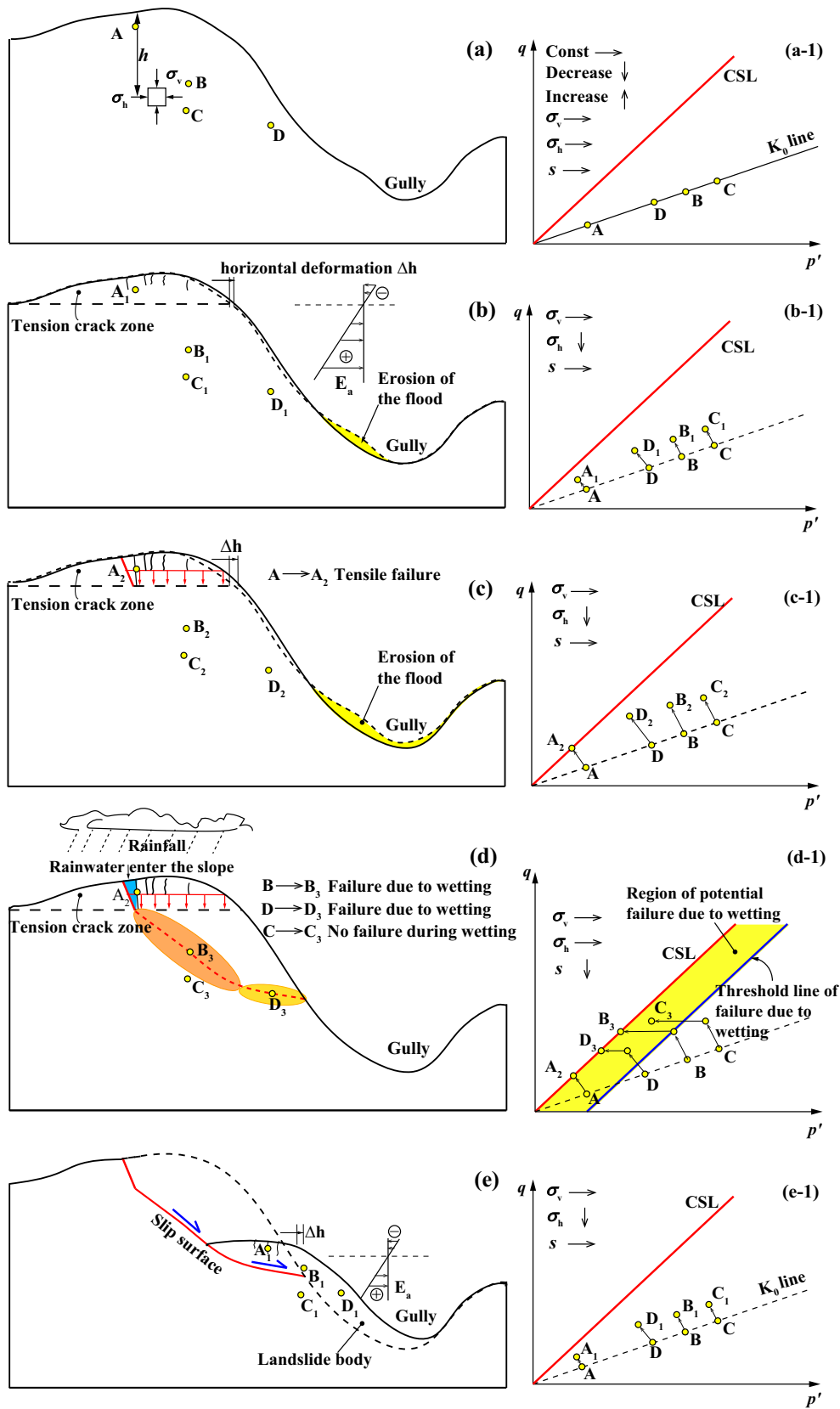


Fig. 16 Formation and evolution process of sliding surface. a Natural state of slope; b fissures occur due to erosion in slope foot; c fissures expand; d potential sliding surface is caused by water infiltration and fissures; e sliding

stable conditions to failure. It tended to increase with the stress level at a given net confining pressure.

The studied loess landslide showed a progressive retreat development. The high-free face formed at the leading edge of the slope created favourable conditions for the occurrence of the landslide. The erosion of rainwater caused the formation of tensile cracks at the top of the slope, accelerating the initiation of the landslide. The wetting-induced loess failure was the key to the formation of sliding surfaces. The occurrence of the failure of the loess slope due to wetting was described mainly in four stages: crack formation and enlarging due to erosion in slope foot, failure of the loess induced by water infiltration through the cracks, expansion of the failure zone due to wetting and formation of the through-sliding surface.

Acknowledgements

The authors want to express their deep thanks to the anonymous reviewers for their constructive comments.

Funding information

This study received financial support from research grants no. 41630639 provided by the National Natural Science Foundation of China, no. 2018YFC1504703 provided by the National Key Research and Development Plan, and no. 2018M633559 provided by the Certificate of China Postdoctoral Science Foundation.

References

- Brand EW (1981) Some thoughts on rainfall induced slope failures. Proceedings of the 10th International Conference on Soil Mechanics and Foundation Engineering, A.A. Balkema, Brookfield, Vt., pp 373–376
- Chen H, Lee CF, Law KT (2004) Causative mechanisms of rainfall-induced fill slope failures. *J Geotech Geoenviron* 130(6):593–602
- Chen CL, Zhang DF, Dong YZ et al (2014) Suction and mechanical behaviours of unsaturated intact loess from constant water content triaxial tests. *Chin J Geotech Eng* 36(7):1195–1202
- Chen CL, Zhang DF, Zhang J, Zhang WB (2017) Compression and wetting deformation behavior of intact loess under isotropic stresses. *Chin J Rock Mech Eng* 36(7):1736–1747
- Chen G, Meng X, Qiao L, Zhang Y, Wang S (2018) Response of a loess landslide to rainfall: observations from a field artificial rainfall experiment in Bailong River basin, China. *Landslides* 15(5):895–911
- Chu J, Leroueil S, Leong WK (2003) Unstable behavior of sand and its implication for slope stability. *Can Geotech J* 40(5):873–885
- Derbyshire E, Meng XM, Kemp RA (1998) Provenance, transport and characteristics of modern aeolian dust in western Gansu Province, China, and interpretation of the quaternary loess record. *J Arid Environ* 39(3):497–516
- Fan XM, Xu Q, Scaringi G et al (2017) A chemo-mechanical insight into the failure mechanism of frequently occurred landslides in the loess plateau, Gansu Province, China. *Eng Geol* 228:337–345
- Farooq K, Orense R, Towhata I (2004) Response of unsaturated sandy soils under constant shear stress drained condition. *Soils Found* 44(2):1–13
- Gallipoli D, Gens A, Sharma R, Vaunat J (2003) An elasto-plastic model for unsaturated soil incorporating the effects of suction and degree of saturation on mechanical behaviour. *Geotechnique* 53(1):123–135
- Gao GR (1988) Formation and development of the structure of collapsing loess in China. *Eng Geol* 25(2–4):235–245
- Hilf JW (1956) An investigation of pore water pressure in compacted cohesive soils. Technical Memo 654, Denver, Bureau of Reclamation
- Khalili N, Khabbaz MH (1998) A unique relationship for the determination of the shear strength of unsaturated soils. *Geotechnique* 48(5):681–687
- Lade PV (1993) Initiation of static instability in the submarine Nerlerkberm. *Can Geotech J* 30(6):895–904
- Lin ZG (2008) Loess in China and landslides in loess slopes. Proceedings of the 10th International Symposium on Landslides and Engineered slopes, Xi'an
- Lin ZG, Wang SJ (1988) Collapsibility and deformation characteristics of deep-seated loess in China. *Eng Geol* 25(2–4):271–282
- Liu D (1985) Loess and environment. Scientific Press, Beijing
- Lourenço SDN, Wang GH, Sassa K, Fukuoka H (2006) Volumetric behavior of saturated sands under poor drainage conditions. *J Geophys Res* 111(F3):187–201
- Maatouk A, Leroueil S, Rochelle P (1995) Yielding and critical state of a collapsible unsaturated silty soil. *Geotechnique* 45(3):465–477
- Nuth M, Laloui L (2008) Effective stress concept in unsaturated soils: clarification and validation of a unified framework. *Int J Numer Anal Methods Geomech* 32(7):771–801
- Oka F, Kodaka T, Suzuki H et al (2010) Experimental study on the behavior of unsaturated compacted silt under triaxial compression. *Soils Found* 50(1):27–44
- Romero E, Vecchia GD, Jommi C (2011) An insight into the water retention properties of compacted clayey soils. *Geotechnique* 61(4):313–328
- Sasitharan S, Robertson PK, Segoo DC, Morgenstern NR (1994) State-boundary surface for very loose sand and its practical implications. *Can Geotech J* 31(3):321–334
- Sassa K, Wang G, Fukuoka H (2003) Performing undrained shear tests on saturated sands in a new intelligent type of ring-shear apparatus. *Geotech Test J* 26(3):257–265
- Sorbino G, Nicotera MV (2013) Unsaturated soil mechanics in rainfall-induced flow landslides. *Eng Geol* 165:105–132
- Take WA, Bolton MD, Wong PCP, Yeung FJ (2004) Evaluation of landslide triggering mechanisms in model fill slopes. *Landslides* 1(3):173–184
- Wang NQ, Luo DH (2010) Freezing effect on loess slope and its stability response. *J Eng Geol* 18(5):103–108
- Wang JD, Zhang ZY (1999) A study on the mechanism of high-speed loess landslide induced by earthquake. *Chin J Geotech Eng* 21(6):670–674
- Wang Q, Pufahl DE, Fredlund DG (2002) A study of critical state on an unsaturated silty soil. *Can Geotech J* 39(1):213–218
- Wang GH, Suemine A, Furuya G, Kaibori M, Sassa K (2005) Rainstorm-induced landslides at Kisawa village, Tokushima Prefecture, Japan, August 2004. *Landslides* 2(3):235–242
- Wang GH, Suemine A, Schulz WH (2010) Shear-rate-dependent strength control on the dynamics of rainfall-triggered landslides, Tokushima prefecture, Japan. *Earth Surf Process Landf* 35(4):407–416
- Wang JJ, Liang Y, Zhang HP, Wu Y, Lin X (2014a) A loess landslide induced by excavation and rainfall. *Landslides* 11(1):141–152
- Wang GH, Zhang DX, Furuya G, Yang J (2014b) Pore-pressure generation and fluidization in a loess landslide triggered by the 1920 Haiyuan earthquake, China: a case study. *Eng Geol* 174:36–45
- Wang JD, Gu TF, Xu YJ (2017) Field tests of expansive soil embankment slope deformation under the effect of the rainfall evaporation cycle. *Appl Ecol Environ Res* 15(3):343–357
- Wang JD, Xu YJ, Ma Y, Qiao S, Feng K (2018) Study on the deformation and failure modes of filling slope in loess filling engineering: a case study at a loess mountain airport. *Landslides* 15(12):2423–2435
- Wang JD, Gu TF, Zhang MS, Xu YJ (2019a) Experimental study of loess disintegration characteristics. *Earth Surf Process Landf*. <https://doi.org/10.1002/esp.4575>
- Wang JD, Li P, Gu Q, Xu YJ, Gu TF (2019b) Changes in tensile strength and microstructure of loess due to vibration. *J Asian Earth Sci* 169:298–307
- Wheeler SL (1988) The undrained shear strength of soils containing large gas bubbles. *Geotechnique* 38(3):399–413
- Xu QJ, Zhang LM (2010) The mechanism of a railway landslide caused by rainfall. *Landslides* 7(2):149–156
- Xu L, Dai FC, Gong QM, Tham LG, Min H (2012) Irrigation-induced loess flow failure in Heifangtai Platform, North-West China. *Environ Earth Sci* 66(6):1707–1713
- Xu L, Dai FC, Tu XB, Tham LG, Zhou YF, Iqbal J (2014) Landslides in a loess platform, North-west China. *Landslides* 11(6):993–1005
- Zhan LT, Chen R, Ng CWW (2014) Wetting-induced softening behavior of an unsaturated expansive clay. *Landslides* 11(6):1051–1061
- Zhang M, Liu J (2010) Controlling factors of loess landslides in western China. *Environ Earth Sci* 59(8):1671–1680

-
- Zhang DX, Wang GH (2007) Study of the 1920 Haiyuan earthquake-induced landslides in loess (China). *Eng Geol* 94(1–2):76–88
- Zhang ZH, Zhang ZY, Wang YS (1987) Basic geologic problems of loess in China. *Acta Geologica Sinica-English Edition* 1(2):362–374
- Zhang DX, Wang GH, Luo CY, Chen J, Zhou YX (2009) A rapid loess flowslide triggered by irrigation in China. *Landslides* 6(1):55–60
- Zhang FY, Liu G, Chen W, Liang S, Chen R, Han W (2012) Human-induced landslide on a high cut slope: a case of repeated failures due to multi-excavation. *J Rock Mech Geotech Eng* 4(4):367–374
- Zhang FY, Wang G, Kamai T, Chen W, Zhang D, Yang J (2013) Undrained shear behavior of loess saturated with different concentrations of sodium chloride solution. *Eng Geol* 155(6):69–79
- Zhang FY, Pei XJ, Chen WW, Liu G, Liang S (2014) Spatial variation in geotechnical properties and topographic attributes on the different types of shallow landslides in a loess catchment, China. *Eur J Environ Civ Eng* 18(4):470–488
- Zhang FY, Kang C, Chan D, Zhang X, Pei X, Peng J (2017) A study of a flowslide with significant entrainment in loess areas in China. *Earth Surf Process Landf* 42(14):326–337
- Zhao HF, Zhang LM (2014) Instability of saturated and unsaturated coarse granular soils. *J Geotech Geoenviron* 140(1):25–35
- Zhou YF, Tham LG, Yan WM, Dai FC, Xu L (2014) Laboratory study on soil behavior in loess slope subjected to infiltration. *Eng Geol* 183:31–38
- Zhu JH, Anderson SA (1998) Determination of shear strength of Hawaiian residual soil subjected to rainfall-induced landslides. *Geotechnique* 48(1):73–82
-
- J. Wang · D. Zhang** (✉) · **T. Gu**
State Key Laboratory of Continental Dynamics, Department of Geology,
Northwest University,
Xi'an, 710069, China
Email: dfzhang87@nwu.edu.cn
- J. Wang**
e-mail: wangjd@nwu.edu.cn
- T. Gu**
e-mail: gutf@nwu.edu.cn
- N. Wang**
College of Geology and Environment,
Xi'an University of Science and Technology,
Xi'an, 710054, China
e-mail: younglock@163.com